World Journal of Surgical Oncology

RESEARCH

Open Access

High expression of HECW1 is associated with the poor prognosis and cancer progression of gastric cancer

Zhihui Yang[1†], Peng Zhou[2†], Liping Wang[1†], Xiao Yang[1], Mengqi Yang[2] and Jiazeng Xia[1,2,3*]

Abstract

Background The E3 ubiquitin ligase HECW1 was found to be involved in ubiquitination modifications during malignant progression of multiple tumors. However, the prognostic role of HECW1 expression in gastric cancer (GC) remains unclear.

Methods The Tumor Immunoassay Resource (TIMER2.0) system evaluated the association of HECW1 with tumor-infiltrating lymphocytes in carcinomas. The UALCAN assessed HECW1 mRNA expression levels in GC tissues and examined their associations with clinicopathological characteristics. The Kaplan Meier-plotter analyzed the effect of HECW1 on the survival of GC patients. The cBioPortal retrieved information about genetic variants in HECW1 gene. Protein–protein interaction (PPI) networks associated with HECW1 were explored using the STRING database. The functional effects of HECW1 on GC cells were evaluated through proliferation (Cell Counting Kit-8), apoptosis (Flow cytometry), and migration (Transwell and wound healing assays). The RNA-Seq was applied to explore the underlying mechanisms.

Results HECW1 demonstrated significant overexpression in GC tumor tissues, correlating with adverse clinical outcomes. Clinically, elevated HECW1 expression exhibited an inverse association with tumor-infiltrating $CD8^+$ T lymphocytes while demonstrating a positive correlation with macrophages, DCs, and neutrophils infiltration, suggesting its potential involvement in tumor immune evasion mechanisms. Functional validation revealed that HECW1 knockdown markedly suppressed GC cell proliferation and migratory capacity, concurrently promoting apoptotic cell death. Mechanistic investigations identified that HECW1 exerts its oncogenic effects through dysregulation of the Hippo signaling pathway, with its silencing effectively attenuating tumor progression via pathway modulation.

Conclusions HECW1 upregulation is significantly associated with poor prognosis and immune infiltration in GC patients, emphasizing its potential as a prognostic biomarker.

Keywords HECW1, Gastric cancer, Immune infiltration, Hippo signaling pathway

†Zhihui Yang, Peng Zhou and Liping Wang contributed equally to this work.

*Correspondence:
Jiazeng Xia
xjz_wuxi@alumni.sjtu.edu.cn

[1]Department of General Surgery, Institute of General Surgical Research, Jiangnan University Medical Center (Wuxi No.2 People's Hospital), School of Medicine, Wuxi, China
[2]Department of General Surgery, People's Hospital of Nanjing Medical University, Wuxi, China
[3]Department of General Surgery, Institute of General Surgical Research, Jiangnan University Medical Center, 68 Zhongshan Lu, Wuxi 214002, P.R. China

Introduction

Gastric cancer (GC) is highly aggressive and metastatic and ranks among the leading causes of cancer-related mortality worldwide [1, 2]. Despite advances in surgical techniques and targeted therapies, progress has been made in the diagnosis and treatment of gastric cancer, but the prognosis of patients with advanced gastric cancer is still poor. Therefore, a deep understanding of the biological mechanisms underlying the development of GC is essential for the designing novel therapeutic interventions.

The E3 ubiquitin ligase, which has the function of determining substrate specificity, plays a decisive role in the ubiquitination process [3, 4]. E3 ubiquitin ligases mainly catalyze the formation of covalent bonds between ubiquitin molecules and specific amino acid residues on target proteins to achieve ubiquitination modifications, with lysine being the most common target for ubiquitination [5]. The HECT-domain ligase HECW1, initially implicated in familial amyotrophic lateral sclerosis pathogenesis [6], demonstrates multifaceted tumor-modulatory functions. Mechanistic studies revealed its catalytic activity-independent regulation of p53-mediated apoptosis [7] and NCOA4-driven ferroptosis in gliomas [8]. Emerging evidence further identified HECW1-mediated suppression of Wnt/β-catenin signaling as a growth inhibitory pathway in cervical carcinogenesis [9]. Nevertheless, the pathophysiological role and molecular targets of HECW1 in GC remain unexplored, warranting systematic investigation.

In this study, the expression, prognostic value, and function of HECW1 were systematically analyzed using bioinformatics databases. Moreover, our results demonstrated that HECW1 knockdown inhibited GC cell proliferation and migration by regulating the Hippo signaling pathway. Our findings elucidate the significance of HECW1 in GC progression and identify HECW1 as a novel prognostic factor. These results suggest HECW1 may serve as a potential therapeutic target for GC.

Materials and methods

Cell culture and management

Human GC cell lines (AGS, MKN-45, MKN-28, MKN-27) and healthy gastric mucosal epithelial cells (GES-1) were purchased from Shanghai Fuheng Biotechnology Corporation. Cell culture was performed in RPMI-1640 medium (Hyclone, USA, sh30809.1) containing 10% fetal bovine serum (MeisenCTCC, USA, CTCC-002-071-50) and 1% penicillin-streptomycin (Gibco, USA, 15140122) at 37 °C with a CO_2 concentration of 5%.

Cell transfection

HECW1 siRNA, HECW1-overexpressing plasmid, and YAP overexpression plasmid was obtained from Azenta, with the following sequences:

Human Negative control sense: UUCUCCGAACGUG UCACGU;

Human Negative control antisense: ACGUGACACGU UCGGAGAA;

Human HECW1 si-1 sense: CAGCUGCAAUUCCGA UUUGTT;

Human HECW1 si-1 antisense: CAAAUCGGAAUUG CAGCUGTT;

Human HECW1 si-2 sense: GAUGAGGUCUUGUCC GAAATT;

Human HECW1 si-2 antisense: UUUCGGACAAGAC CUCAUCTT.

Cells in the logarithmic growth phase were seeded onto plates to achieve 40–60% confluence by the next day. Transfection with siRNA was then performed using jetPRIME® (Polyplus, France; 101000046). The culture medium was replaced with fresh medium within 24 h post-transfection. Transfection efficiency was evaluated at 48 h post-transfection via quantitative real-time PCR (qRT-PCR) and Western blot analysis. Verteporfin was purchased from MCE (Catalog No. HY-B0146).

RNA extraction and qRT-PCR

We used FastPure Cell/Tissue Total RNA Isolation Kit V2 (vazyme, China, RC112-01) to extract RNA from GC tissues and GC cells. Reverse transcription was performed using HiScript ® III all in one RT SuperMix for qPCR (vazyme, China, R333-01). qRT-PCR was performed using the ChamQ universal SYBR qPCR Master Mix kit (vazyme, China, Q711-02). The specific primers used are listed below.

Human GAPDH forward primer: GAAGGTGAAGGT CGGAGTC;

Human GAPDH reverse primer: GAAGATGGTGATG GGATTTC;

Human HECW1 forward primer: GCAGTTTGTCAC GGGAACAT;

Human HECW1 reverse primer: GGAAGATCCAGTC GGTTGAA.

CCK-8 assays

Cell counting kit-8 (CCK8) (beyotime, China, C0037) was used to detect the proliferation of GC cells. $3*10^3$ cells were inoculated into 96-well plates, and 10 μl of CCK8 and 90ul of serum-free medium mix were added to each well and injected every 24 h. After incubation for 2 h, absorbance values were recorded at 450 nm using an enzyme-labeled instrument (Thermo Scientific, MA, USA).

Transwell assay

24 h after transfection of the cells, the cells were diluted to $1*10^6$ cells/mL with serum-free 1640 medium and 200 μL was taken and added to the transwell chambers. Then 500μL of 1640 medium containing 10% FBS was added to the transwell lower chamber. After incubation for 24 h, the cells were fixed with methanol and stained with crystal violet. Finally, the photographs were observed with an inverted microscope (Olympus, Tokyo, Japan).

Western blot assay

Total proteins from transfected GC cells were extracted with RIPA lysate (Beyotime, China, P0013B) containing 1% PMSF (Solarbio, China, P0100). protein concentration was detected by BCA kit (Beyotime, China, P0012). Protein samples were separated by electrophoresis using 10% Precast Protein Plus Gel (Yeasen, China, 36276ES10) and then transferred to PVDF membrane (Millipore, USA, ISEQ00010). The membrane was closed with rapid closure solution (Ncmbio, China, P30500) for 30 min, and then incubated with β-actin (CST, USA, 4967 S), HECW1(Proteintech, China, 24695-1-AP), YAP antibody (CST, USA, 14074T) and p-YAP (Affinity, China, AF3328), which were diluted at 1:1000, at 4 °C overnight. The next day, the membrane was washed four times (5 min each) with TBST and then incubated with HRP-conjugate Mouse Anti-Rabbit IgG Antibody (CST, USA, 7076P2) which was diluted at 1:5000, at room temperature for 2 h. After incubation, the washing was repeated. Bands were then measured by a chemiluminescence imaging device (Bio-Rad, California, USA) using an ECL detection kit (Beyotime, China, P0018S). β-actin was used as an internal reference.

Immune infiltration analysis

TIMER 2.0 [10] is an online database that can be used to analyze immune infiltration in different cancer types [11], including cancer-associated fibroblasts (CAFs), B cells, $CD4^+$ T cells, $CD8^+$ T cells, neutrophils, macrophages and dendritic cells (DCs). We analyzed the expression of HECW1 in different cancers and the correlation with immune infiltration.

Kaplan-Meier plotter

The Kaplan Meier [12] is capable of assessing the correlation between the expression of all genes and survival in 21 tumor types. Statistical tools applied include Cox proportional hazards regression and misdiagnosis rate calculations. Setting to split patients by median with a follow-up threshold of 60 months.

Gene co-expression analysis

Gene Expression Profiling Interactive Analysis (GEPIA2) is an online database of 60,498 genes and 198,619 isoforms of type [13]. We analyzed the association between HECW1 expression and marker genes of tumor-infiltrating immune cells (mainly T cells, TAM, macrophages, NK cells, DC cells, T helper cells and neutrophils) using data from the TCGA and GTEx projects in conjunction with RNA sequencing expression analysis. Correlation coefficients were determined using the Spearman method.

Genetic variation

We retrieved HECW1 gene alterations through cBioPortal [14] and studied them in 33 cancers. The Mutation Module provides HECW1 mutation sites to improve the understanding of its potential role in GC development.

Flow cytometry

Cells (1×10^6 – 3×10^6) were collected, centrifuged, and washed twice with pre-chilled PBS. The pellet was resuspended in 500 μl Apoptosis Positive Control Solution (Liankebio, China; Cat# AT107) and incubated on ice for 30 min. After centrifugation and PBS washing, cells were resuspended in 500 μl 1× Binding Buffer. Annexin V-APC (5 μl) and PI (10 μl) were added to each tube, followed by gentle vortexing and a 5-minute incubation at room temperature in the dark. Apoptosis analysis was performed immediately using a flow cytometer (Beckman Coulter, USA), with data processed by FlowJo 10 software.

Co-culture of cancer cells and T cells

The peripheral blood from health donors were provided by Surgery Department of Wuxi No.2 People's Hospital. The peripheral blood mononuclear cells (PBMC) was isolated from the peripheral blood with Lymphoprep (STEMCELL, Canada, 19654) and activated with ImmunoCult Human CD3/CD28 T Cell Activator (STEMCELL, Canada, 100–0784) in ImmunoCult-XF T Cell Expansion Medium (STEMCELL, Canada, 10981) supplemented with IL2. Pre-activated $CD8^+$ T cells were washed with PBS, resuspended in fresh complete medium, and co-cultured with GC cells transfected with specified plasmids in 48-well plates at an optimized effector-to-target ratio. The co-culture system was maintained for 48 h under standard conditions (37 °C, 5% CO_2). Following co-culture, T cells were harvested and treated with protein transport inhibitor (BD) for 6 h at 37 °C to accumulate intracellular cytokines. Cells were subsequently fixed and permeabilized using the BD Cytofix/Cytoperm™ Kit (554714) according to the manufacturer's protocol. Intracellular staining was performed with fluorochrome-conjugated antibodies targeting IFN-γ (Miltenyi Biotec, 130-113-497) and TNF-α (Miltenyi Biotec, 130-118-974). Data acquisition was conducted using a Beckman CytoFlex flow cytometer, and quantitative analysis was performed with FlowJo software.

RNA-Seq analysis

Total RNAs were extracted from both si-HECW1 and si-Ctrl samples. We employed RNA-Seq technology (Novogene, China) for the identification of DEGs (Differentially Expressed Genes) [15]. Briefly, the raw fastq data generated from RNA-seq was first trimmed using Trimmomatic (V0.35). The trimmed reads were then compared to the human reference genome (NCBI GRCh38) by utilizing TopHat (version 2.0.12) and default parameter settings. The resulting aligned bam files were then processed using Cufflinks (Version 2.2.1) for gene quantification. Genes meeting the threshold of FPKM ≥ 1 (Fragments Per Kilobase of transcript per Million mapped reads) across all samples were included in the subsequent analysis to identify DEGs. The R Bioconductor package DESeq2 was utilized to screen out the differentially expressed genes (DEGs). The *P* value for correction < 0.05 and fold change > 2 or < 0.5 were set as the cut-off criteria for identifying DEGs.

Statistics

Statistical differences were analyzed using GraphPad Prism 9 software. The data is displayed as the mean ± standard error of the mean (SEM). For enrichment analysis, R 4.4.0 were utilized. To examine the variations between the two groups, the student's t-test was employed. $p < 0.05$ was recognized statistically significant.

Results

HECW1 is over-regulated and associated with survival in gastric cancer

The pan-cancer expression profile of HECW1 was initially retrieved through the TIMER 2.0 database, demonstrating significantly elevated expression levels in stomach adenocarcinoma (STAD) compared with paired adjacent normal tissues (Fig. 1A). Subsequent validation using the UALCAN platform [16] confirmed HECW1 mRNA overexpression in GC clinical specimens versus normal controls (Fig. 1B). Comparative analysis revealed upregulated HECW1 expression in GC cell lines (HGC-27, MKN-28,

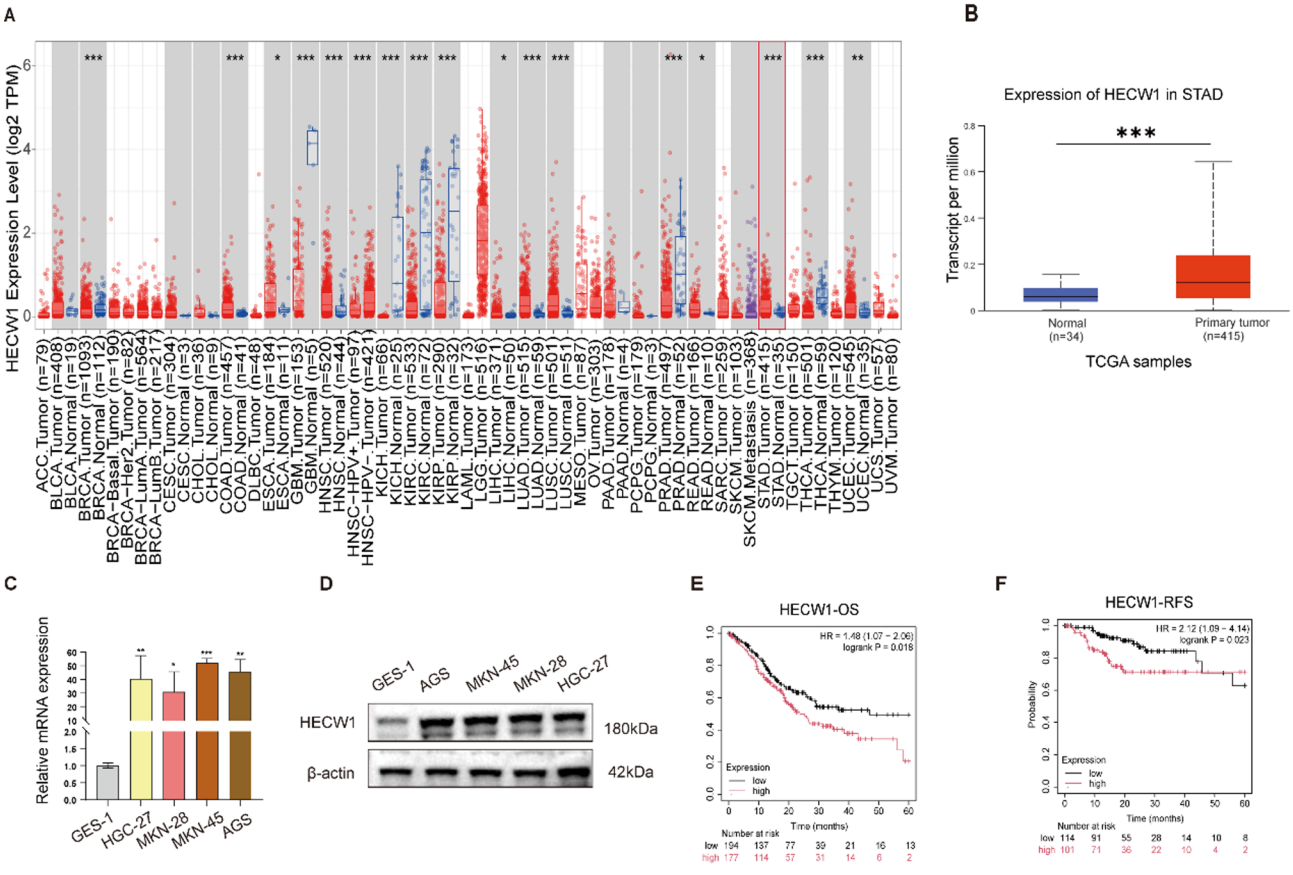

Fig. 1 Dysregulated expression pattern of HECW1 in gastric cancer. **(A)** Pan-cancer analysis using TIMER2.0 database revealed significantly aberrant HECW1 expression in GC tissues compared with normal controls. **(B)** Validation through UALCAN platform confirmed HECW1 upregulation in GC clinical specimens. **(C)** Comparative analysis of HECW1 mRNA levels between normal gastric epithelial cells (GES-1) and four GC cell lines (HGC-27, MKN-28, MKN-45, AGS) by qRT-PCR. **(D)** Western blot analysis demonstrating elevated HECW1 protein expression in GC cell lines compared with GES-1. **(E-F)** Prognostic significance of HECW1 expression in STAD cohort from Kaplan-Meier Plotter database: **(E)** Overall survival (OS, $n = 375$ patients) and **(F)** relapse-free survival (RFS, $n = 375$ patients). $^{*}p < 0.05$, $^{**}P < 0.01$, $^{***}P < 0.001$

MKN-45, AGS) relative to normal gastric epithelial cells (GES-1), with transcriptional activation confirmed by qRT-PCR (Fig. 1C) and protein overexpression validated by Western blot (Fig. 1D). Prognostic evaluation via Kaplan-Meier Plotter [12] identified HECW1 overexpression as a negative predictor for both overall survival (OS; HR = 1.48, log-rank $P = 0.018$) and relapse-free survival (RFS; HR = 2.12, log-rank $P = 0.023$) in STAD patients (Fig. 1E-F). Multivariate Cox regression analysis of TCGA-STAD data established HECW1 expression (HR = 1.649, 95% CI = 1.045–2.603, $P = 0.032$) and advanced age (> 65 years) (HR = 1.701, 95% CI = 1.068–2.710, $P = 0.025$) as independent prognostic factors for GC (Table 1).

Association of HECW1 expression with clinicopathologic characteristics

The relationship between HECW1 mRNA expression and clinical parameters in STAD was assessed by UALCAN, which is a comprehensive and interactive web resource for analyzing TCGA transcriptome and clinical patient data based on TPM normalization. The results showed that HECW1 was differentially expressed in patients of individual cancer stages, race, gender, age, tumor grade, *H. pylori* infection status, histological subtypes, nodal metastasis status, and TP53 mutation status (Fig. 2A-I).

Table 1 Univariate and multivariate Cox regression analyses of the overall survival of GC

Characteristics	Total(*N*)	Univariate analysis		Multivariate analysis	
		Hazard ratio (95% CI)	*P* value	Hazard ratio (95% CI)	*P* value
Pathologic T stage	362				
T1&T2	96	Reference		Reference	
T3	167	1.713 (1.103 - 2.660)	**0.016**	1.495 (0.817 - 2.736)	0.192
T4	99	1.729 (1.061 - 2.819)	**0.028**	1.206 (0.584 - 2.488)	0.613
Pathologic N stage	352				
N0	107	Reference		Reference	
N1	97	1.629 (1.001 - 2.649)	**0.049**	0.947 (0.483 - 1.856)	0.874
N2	74	1.655 (0.979 - 2.797)	0.060	1.033 (0.519 - 2.055)	0.926
N3	74	2.709 (1.669 - 4.396)	**< 0.001**	1.746 (0.905 - 3.366)	0.096
Gender	370				
Female	133	Reference			
Male	237	1.267 (0.891 - 1.804)	0.188		
Race	320				
Asian	73	Reference			
Black or African American	11	1.949 (0.808 - 4.698)	0.137		
White	236	1.449 (0.873 - 2.405)	0.152		
Age	367				
<= 65	163	Reference		Reference	
> 65	204	1.620 (1.154 - 2.276)	**0.005**	1.701 (1.068 - 2.710)	**0.025**
Histologic grade	361				
G1	10	Reference			
G2	134	1.648 (0.400 - 6.787)	0.489		
G3	217	2.174 (0.535 - 8.832)	0.278		
Reflux history	213				
No	174	Reference		Reference	
Yes	39	0.582 (0.291 - 1.162)	0.125	0.602 (0.268 - 1.350)	0.218
H pylori infection	162				
No	144	Reference			
Yes	18	0.650 (0.279 - 1.513)	0.317		
Barretts esophagus	207				
No	192	Reference			
Yes	15	0.892 (0.326 - 2.441)	0.824		
Pathologic M stage	352				
M0	327	Reference		Reference	
M1	25	2.254 (1.295 - 3.924)	**0.004**	2.040 (0.823 - 5.059)	0.124
HECW1	370				
Low	185	Reference		Reference	
High	185	1.489 (1.068 - 2.076)	**0.019**	1.649 (1.045 - 2.603)	**0.032**

HECW1 gene alterations in GC

Comprehensive genomic profiling of HECW1 alterations was performed through cBioPortal analysis platform using 32 cancer cohorts from The Cancer Genome Atlas (TCGA) Pan-Cancer Atlas ($n = 10{,}967$ tumor samples). The investigation identified 529 somatic alterations spanning the entire HECW1 coding sequence (amino acid positions 1-1606), comprising 444 missense mutations, 58 truncating mutations, 21 splice site variants, 5 gene fusions, and 1 in-frame mutation. A recurrent hotspot

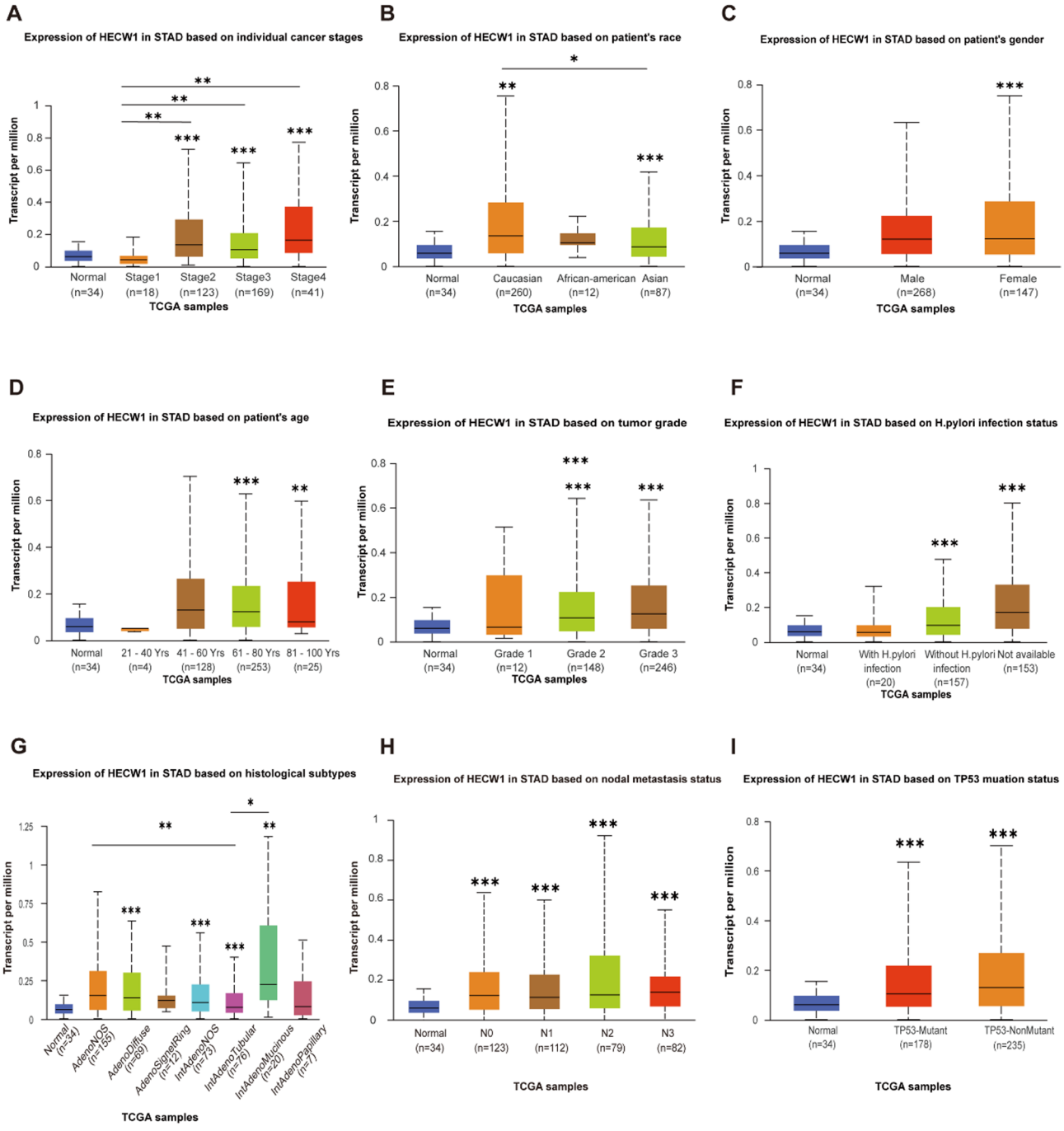

Fig. 2 Association of HECW1 expression and clinical characteristics of STAD. (**A**) Expression of HECW1 in STAD based on individual cancer stages. (**B**) Expression of HECW1 in STAD based on patient's race. (**C**) Expression of HECW1 in STAD based on patient's gender. (**D**) Expression of HECW1 in STAD based on patient's age. (**E**) Expression of HECW1 in STAD based on tumor grade. (**F**) Expression of HECW1 in STAD based on *H.pylori* infection status. (**G**) Expression of HECW1 in STAD based on histological subtypes. (**H**) Expression of HECW1 in STAD based on nodal metastasis status. (**I**) Expression of HECW1 in STAD based on TP53 muation status. *$P < 0.05$, **$P < 0.01$,***$P<0.001$

mutation R1555W (Arg1555Trp) was identified as the most prevalent alteration (Fig. 3B). Notably, STAD exhibited distinct mutation patterns characterized by predominant missense substitutions and gene amplifications (Fig. 3A).

Immunological infiltration of the HECW1 gene is present in gastric cancer

The TIMER 2.0 database was employed to analyze the correlations between HECW1 expression level and immune infiltration in STAD. Multi-algorithm deconvolution (EPIC, MCP-COUNTER, XCELL, TIDE) revealed a positive correlation between HECW1 expression and cancer-associated fibroblast (CAF) infiltration (Fig. 4A) alongside reduced tumor purity in STAD. In GC, elevated HECW1 levels inversely correlated with $CD8^+$ T cell infiltration and promoted macrophages, DCs and neutrophils recruitment (Fig. 4B). These findings suggest that HECW1 may function as a potential immunomodulator driving immunosuppressive niche formation through dysregulation of cytotoxic T cell trafficking and macrophage polarization. Functional validation through PBMC coculture assays demonstrated that HECW1-knockdown GC cells increased $CD3^+CD8^+$ T cell proportions (Fig. 4C) and enhanced IFN-γ/TNF-α secretion (Fig. 4D-E), suggesting its role in modulating T cell activity. GEPIA2 analysis further showed HECW1 co-expression with immune markers (NK cells, DCs, TAMs, etc.) in GC versus normal tissues (Table 2).

Effect of knockdown of HECW1 on the biological behavior of tumors

Following database findings, we validated HECW1's functional role in GC through in vitro experiments. Two independent siRNAs were used to knock down HECW1 in AGS and MKN-45 cells, with knockdown efficiency confirmed by RT-qPCR and Western blot (Fig. 5A-B). Subsequently, we found that the proliferation of GC cells in the low HECW1-expressing group was significantly lower than that of the control group with CCK8 (Fig. 5C). Depletion of HECW1 significantly induced apoptosis in both AGS and MKN-45 via Annexin V/PI assay (Fig. 5D). Additionally, Transwell and Wound

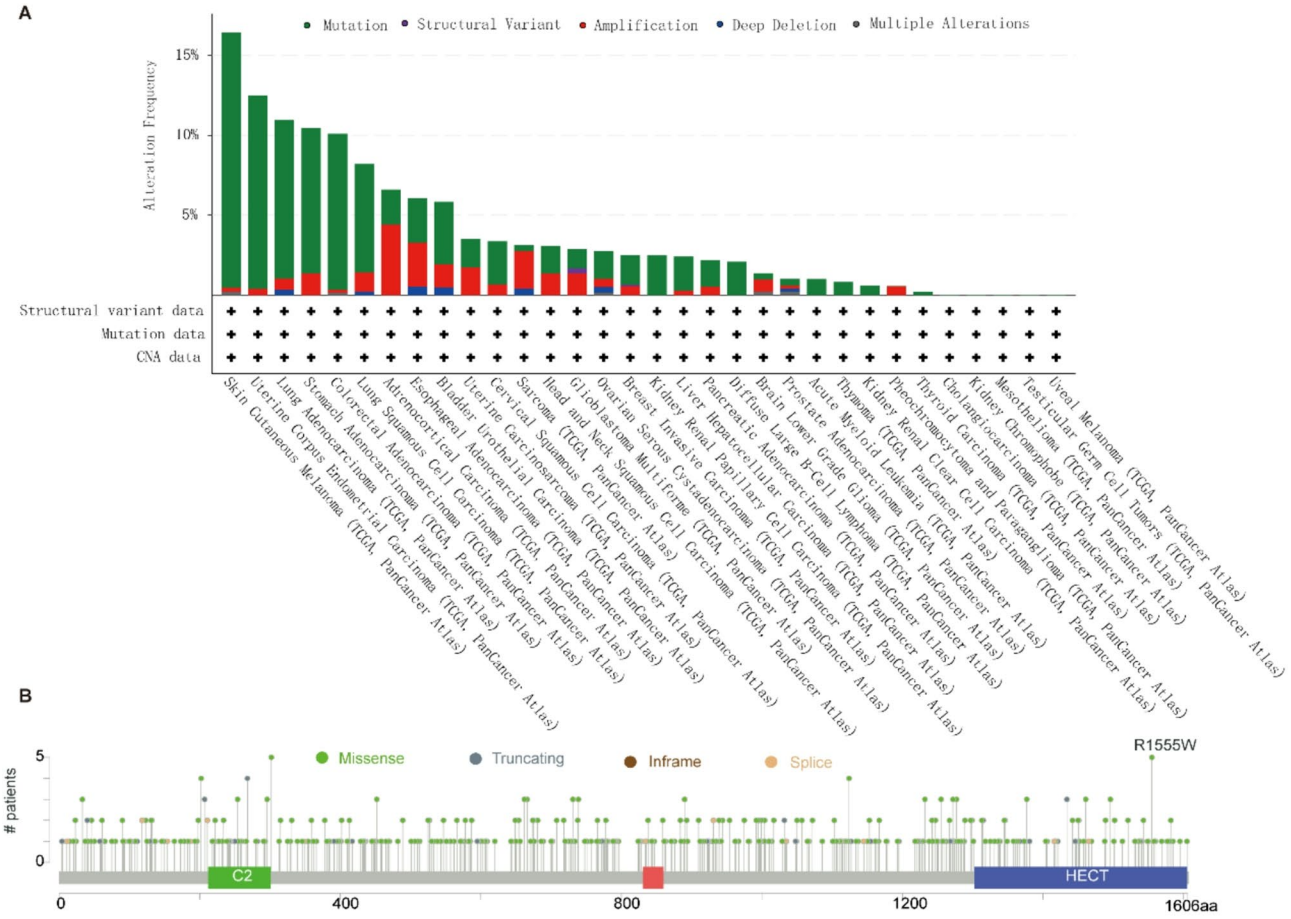

Fig. 3 Genomic landscape of HECW1 alterations across human cancers. **(A)**Histograms of HECW1 mutations in 32 kinds of cancer. **(B)** HECW1 mutation map across protein domains

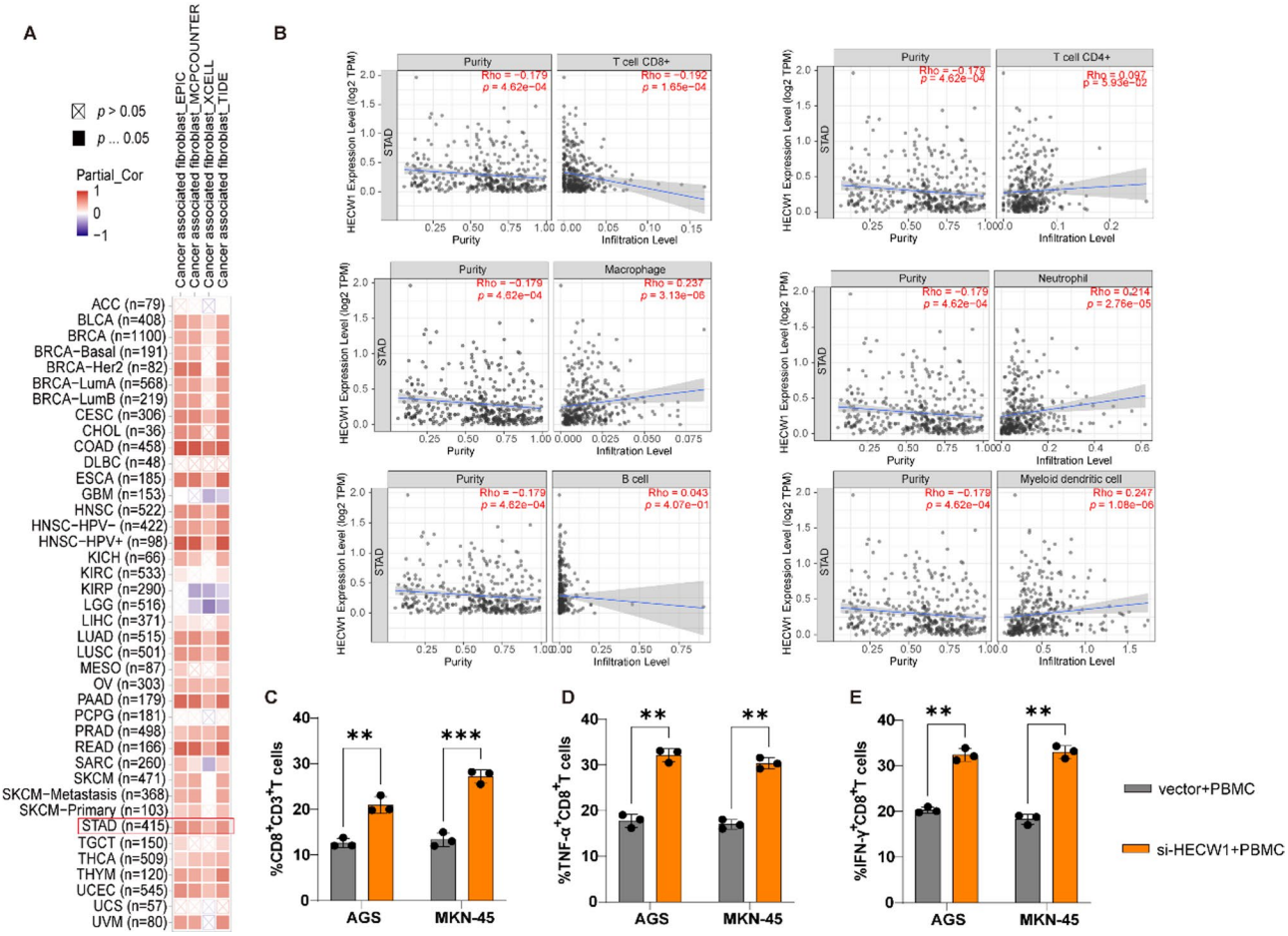

Fig. 4 Immunological infiltration of the HECW1 gene is present in GC. **(A)** The expression level of HECW1 in STAD showed a positive correlation with the infiltration of cancer-associated fibroblasts. **(B)** Analysis of the correlation between HECW1 gene expression levels and immune cell infiltration. **(C)** Statistical quantitation of $CD3^+CD8^+$T cells. **(D)** Statistical quantitation of TNF-α^+CD8^+T cells. **(E)** Statistical quantitation of IFN-γ^+CD8^+T cells. *$P < 0.05$, **$P < 0.01$,***$P<0.001$

Healing assay revealed that migration of GC cells with low HECW1 expression was impaired (Fig. 5E-F).

Gene enrichment analysis of the HECW1 gene in tumors

Protein-protein interaction (PPI) network analysis using the STRING database and Cytoscape identified HECW1-interacting proteins (Fig. 6A). Functional enrichment analysis (GO/KEGG) of these interactors revealed significant associations with ubiquitin-proteasome system regulation and Hippo signaling pathway (Fig. 6B-C). siRNA-mediated HECW1 knockdown in GC cells increased phosphorylated YAP (p-YAP) levels while reducing total YAP expression (Fig. 6D).

Identification of differentially expressed genes and functional enrichment analysis

To further investigate the role of HECW1 in GC and its impact on tumor suppression, RNA-Seq was performed based on si-HECW1 and si-Ctrl group in MKN-45 cells. As the volcano plots illustrated, after data integration, gene expression profiles from RNA Sequencing identified 952 differentially expressed genes. Among all the DEGs, 398 genes were upregulated and 554 were downregulated in si-HECW1 compared with the si-Ctrl in MKN-45 (Fig. 7A), grounded on the cut-off criteria (|logFC|> 2, *P*adj < 0.01). DEGs were selected for integrated analysis. To explore the biology pathways of the DEGs, we performed KEGG analysis for up and down DEGs (Fig. 7B-C). Enriched KEGG pathways of the DEGs were shown in Fig. 7C, including Hippo signaling pathway and some other pathways, which was consistent with the results analyzed above in the public database.

Hippo pathway activation blocks the anti-tumor effects induced by HECW1 knockdown

To validate the HECW1-YAP regulatory axis, we co-transfected HECW1 siRNA with a YAP overexpression plasmid in GC cells. Western blot analysis revealed that HECW1 knockdown significantly increased the protein level of p-YAP, while decreasing the protein levels of

Table 2 Correlations between HECW1 and gene markers of immune cells in GEPIA2

Cell types	Gene markers	SATD			
		Tumor		Normal	
		P	R	P	R
Naïve T-cell	CCR7	6.1e−08	0.22	0.0088	0.18
	LEF1	9.2e−22	0.38	3.5e−06	0.31
	TCF7	3.6e−09	0.24	0.0069	0.19
	SELL	9.4e−15	0.31	4.4e−08	0.37
Effector T-cell	CX3CR1	3.6e−11	0.27	0.0056	0.19
	FCGR3A	8.9e−16	0.32	1.6e−05	0.29
	CD8A	0.021	0.096	3.6e−05	0.28
	CD8B	4e−04	0.15	0.0011	0.22
Effector memory T-cell	PDCD1	5.7e−06	0.19	2e−04	0.25
	DUSP1	0.0047	0.12	0.33	0.068
	GZMK	2.4e−06	0.19	0.00024	0.25
	GZMA	2.4e−06	0.19	3.5e−08	0.37
	IFNG	5.9e−07	0.21	0.00039	0.24
Resident memory T-cell	CD69	0.024	0.094	0.0063	0.19
	ITGAE	0.069	0.075	0.34	0.065
	CXCR6	7.4e−06	0.18	0.0011	0.22
	MYADM	2.7e−17	0.34	0.0078	0.18
Central memory T-cell	CCR7	6.1e−08	0.22	0.0088	0.18
	SELL	9.4e−15	0.31	4.4e−08	0.37
	IL7R	7.6e−07	0.2	0.02	0.16
Exhausted T-cell	HAVCR2	1.4e−14	0.31	1.1e−05	0.3
	GZMB	3.8e−10	0.26	3e−07	0.34
	TIGIT	4.8e−12	0.28	3.6e−05	0.28
	LAG3	3e−06	0.19	2e−05	0.29
	PDCD1	5.7e−06	0.19	2e−04	0.25
	CXCL13	1.4e−08	0.23	0.005	0.19
	LAYN	4.8e−05	0.17	0.33	0.068
Resting Treg	FOXP3	2.5e−16	0.33	1.9e−08	0.38
	IL2RA	6.6e−16	0.33	2.5e−06	0.32
Effector Treg	CTLA4	2.3e−11	0.27	9.8e−06	0.3
	CCR8	1.5e−19	0.36	9.8e−06	0.3
	TNFRSF9	9.9e−19	0.35	5.8e−08	0.36
Th1-like	CXCL13	1.4e−08	0.23	0.005	0.19
	HAVCR2	1.4e−14	0.31	1.1e−05	0.3
	IFNG	5.9e−07	0.21	0.00039	0.24
	CXCR3	1.1e−09	0.25	2e−05	0.29
	BHLHE40	1.2e−11	0.28	0.037	0.14
	CD4	0.5e−15	0.31	2e−09	0.4
	TNF	0.2e−16	0.33	0.00011	0.26
	Tbx21	0.024	0.093	0.0036	0.2
	STAT4	0.002	0.13	0.018	0.16
	STAT1	9.4e−14	0.3	1.2e−06	0.33
Natural killer cell	KIR2DL1	7.2e−08	0.22	0.00089	0.23
	KIR2DL3	1.2e−09	0.25	0.029	0.15
	KIR2DL4	7.1e−07	0.2	1e−06	0.33
	KIR3DL1	4e−06	0.19	0.048	0.14
	KIR3DL2	1.1e−05	0.18	0.0047	0.19
	KIR3DL3	0.0029	0.12	0.11	0.11
	KIR2DS4	0.0021	0.13	0.079	0.12
Th17	STAT3	5.7e−10	0.25	0.071	0.12
	IL17A	9.8e−12	0.28	3.7e−06	0.31

Table 2 (continued)

Cell types	Gene markers	SATD			
		Tumor		Normal	
		P	R	P	R
Th2	GATA3	3.8e−16	0.33	8.6e−09	0.38
	STAT6	0.0091	0.11	0.019	0.16
	STAT5A	1.3e−08	0.23	0.064	0.13
	IL13	0.22	0.051	0.85	−0.013
Dendritic cell	HLA-DPB1	9.1e−10	0.25	5e−09	0.39
	HLA-DQB1	1.2e−06	0.2	0.00013	0.26
	HLA-DRA	1.1e−09	0.25	5.2e−11	0.43
	HLA-DPA1	5.3e−11	0.27	4.2e−10	0.41
	CD1C	8.1e−07	0.2	0.011	0.18
	NRP1	1.1e−15	0.32	0.0097	0.18
	ITGAX	1.4e−14	0.31	0.0023	0.21
TAM	CCL2	4.2e−06	0.19	0.13	0.1
	CD68	1.1e−20	0.37	4.3e−10	0.41
	CD115	5.1e−08	0.22	1e−05	0.3
Neutrophil	CEACAM8	3.8e−09	0.24	0.49	−0.048
	ITGAM	2.5e−09	0.24	0.014	0.17
	CCR7	6.1e−08	0.22	0.0088	0.18
B cell	CD19	4.9e−07	0.21	0.0046	0.19
	CD79A	2.8e−08	0.23	0.00033	0.25
M1 macrophage	NOS2	2.2e−10	0.26	0.014	0.17
	IRF5	7.7e−14	0.3	0.00017	0.26
	PTGS2	2.3e−08	0.23	0.23	0.083
M2 macrophage	CD163	0.79	0.011	0.99	−0.00066
	VSIG4	0.012	0.1	0.037	0.14
	MS4A4A	0.00029	0.15	0.029	0.15

R represents correlation coefficient. P represents P value

YAP and TAZ. However, overexpression of YAP reversed this phenomenon (Fig. 8A). Functional assays demonstrated that HECW1 silencing suppressed proliferation (CCK-8 assay), which was rescued by YAP overexpression (Fig. 8B). Similarly, HECW1 depletion induced apoptosis (Annexin V/PI staining), whereas YAP ectopic expression reversed this phenotype (Fig. 8C). Transwell and wound healing assays confirmed that HECW1 knockdown impaired migration, an effect counteracted by YAP overexpression (Fig. 8D-E). Functional validation through PBMC coculture assays demonstrated that HECW1-knockdown GC cells significantly increased the proportion of $CD3^+CD8^+$ T cells and enhanced IFN-γ and TNF-α secretion. However, overexpression of YAP reversed this effect, indicating that HECW1 modulates T cell activity via the Hippo signaling pathway (Fig. 8F). Verteporfin, a YAP inhibitor, disrupted the YAP/TAZ-TEAD interaction. As shown in Fig. 8G, verteporfin attenuated the upregulated YAP protein expression caused by HECW1 overexpression. These results suggested that HECW1 could regulate the Hippo signaling pathway to promote the malignant progression of GC cell lines.

Discussion

HECW1 promoted metastasis in non-small cell lung cancer by mediating ubiquitination of Smad4 [17]; induced NCOA4-regulated ferroptosis in glioma by ubiquitination and degradation of ZNF350 [8]; and inhibited growth of cervical cancer cells by promoting ubiquitination of DVL1 [9].Our systematic analysis extended these findings to GC, demonstrating significant correlations between HECW1 overexpression and reduced patient survival (log-rank $P = 0.018$, HR = 1.48). Functional interrogation through HECW1 knockdown in GC cell lines demonstrated significant suppression of cellular proliferation, enhanced apoptotic activity, and impaired migratory capacity. These findings collectively indicated that HECW1 critically promotes the malignant progression of gastric carcinoma.

Furthermore, we revealed that HECW1 regulated immune processes. This implied that further exploration of the prognostic value and immunomodulatory function of HECW1 in GC was warranted. Immunotherapy has made a significant impact in the treatment of tumors [18]. The abundance and distribution of tumor-infiltrating lymphocytes (TILs) served as significant

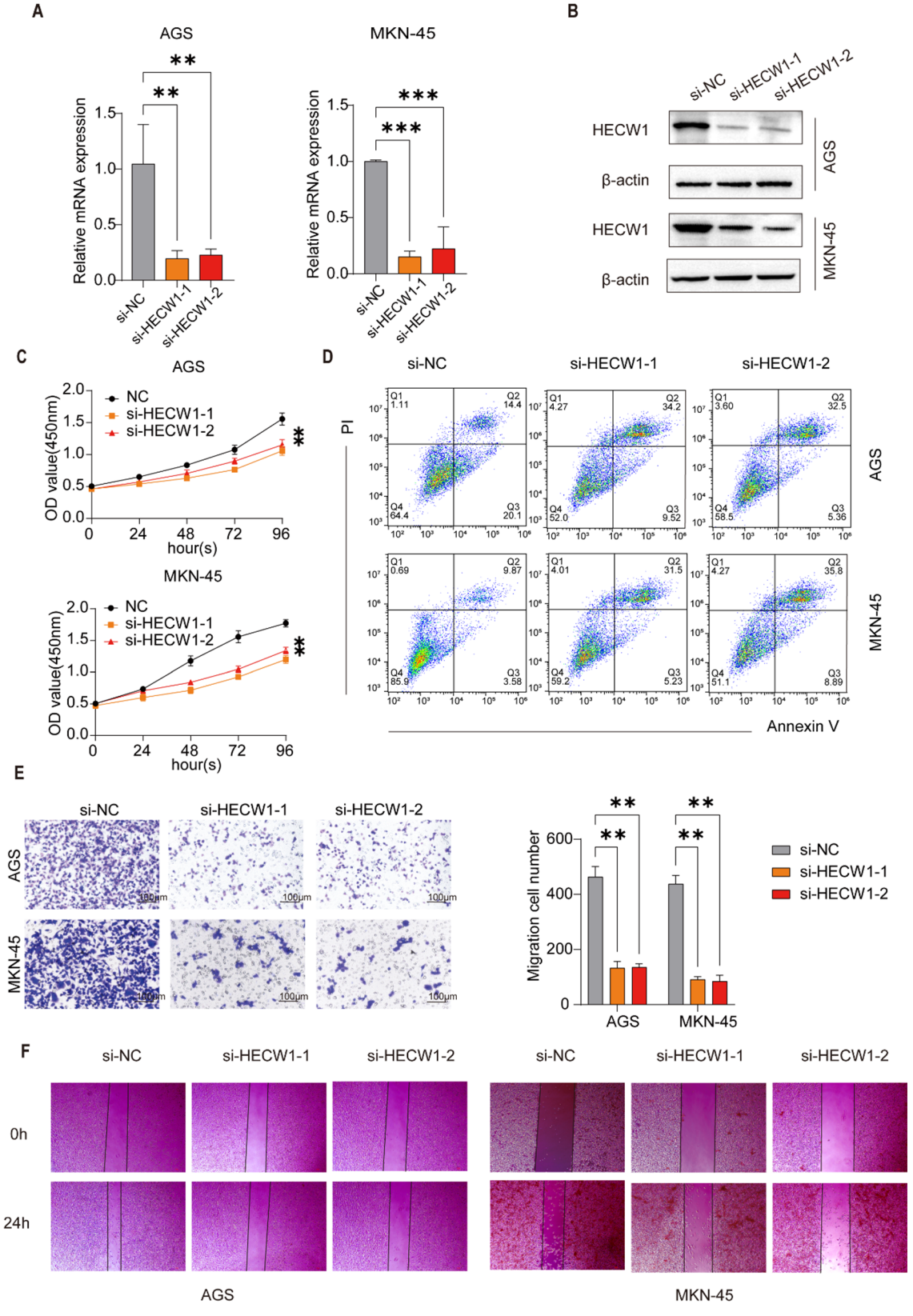

Fig. 5 (See legend on next page.)

(See figure on previous page.)

Fig. 5 High HECW1 Expression in GC Cells. **(A)** The expression of HECW1 was detected by qRT-PCR after HECW1 knockdown. **(B)** The protein of HECW1 was detected by western blot assays. **(C)**The effect of HECW1 on proliferation was verified by Cell Counting Kit-8 after the knockdown of HECW1 in the AGS and MKN-45 cells. **(D)** Annexin V/PI dual staining revealed AGS and MKN-45 increase in apoptotic populations following HECW1 knockdown compared to scramble controls. **(E)** Transwell assays of AGS and MKN-45 cells treated as indicated. **(F)**Wound healing assays were conducted to detect the invasion of these transfected GC cells. Transwell assays were stained by crystal violet solution. Scale bar, **(E)** 100 μm, **(F)** 100 μm. $*p < 0.05$, $**p < 0.01$, $***p < 0.001$

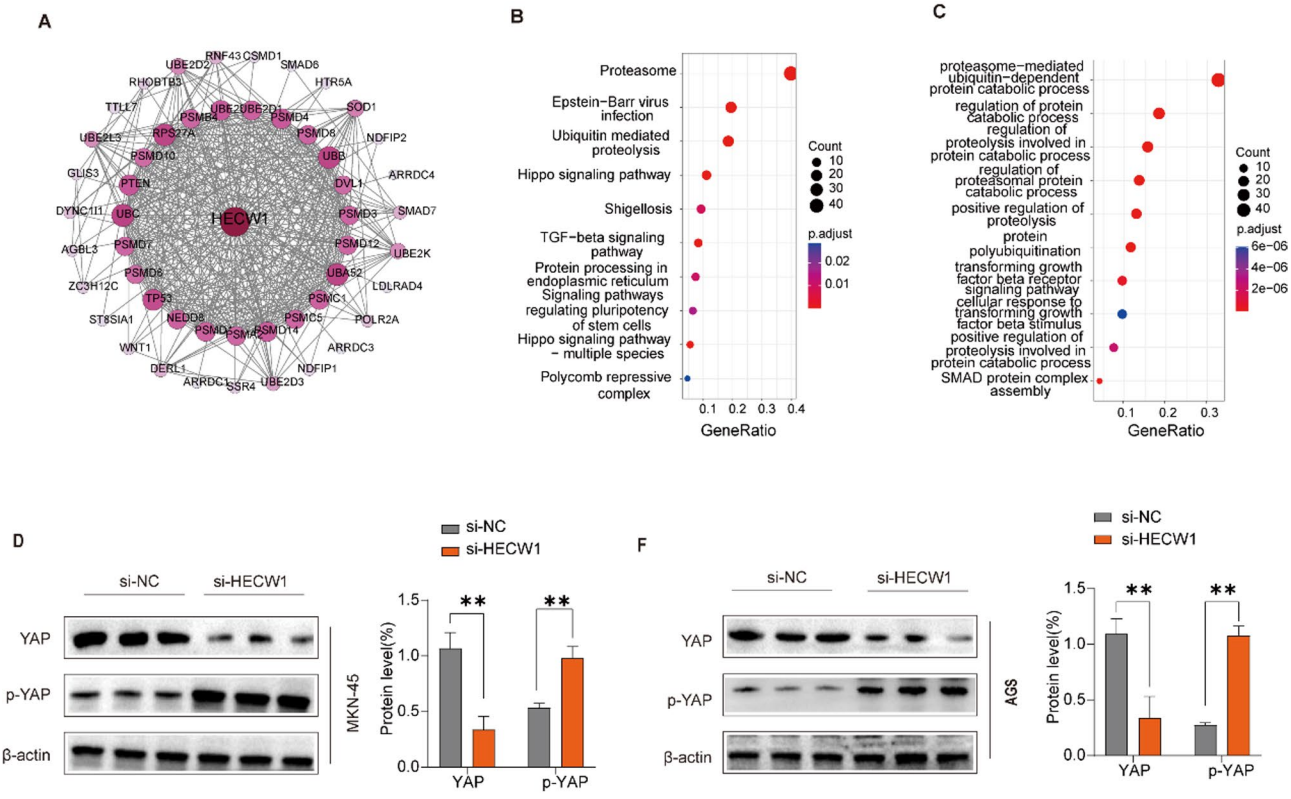

Fig. 6 Gene enrichment analysis of the HECW1 gene in tumors. **(A)**Extraction of STRING database proteins interacting with HECW1 and mapping of PPI networks using Sytoscape processing. **(B)**Enrichment analysis of HECW1 by KEGG. **(C)**Enrichment analysis of HECW1 by GO. **(D)** The protein level of p-YAP and YAP after silencing HECW1 or not (si-NC). $*p < 0.05$, $**p < 0.01$, $***p < 0.001$

biomarkers in the tumor immune microenvironment (TIME), demonstrating close associations with prognosis and responsiveness to immunotherapy [19]. In primary cancers of the gastrointestinal tract, the presence of anti-tumor immune infiltration was often associated with a better prognosis [20].Our study identified HECW1 as a key modulator of tumor immune microenvironment dynamics, critically regulating both the abundance and phenotypic diversity of tumor-infiltrating immune cells. High HECW1 expression inversely correlated with $CD8^+$ T lymphocyte infiltration while showing a positive association with macrophages, DCs, and neutrophils infiltration. $CD8^+$ T cells were the most important anti-tumor effector cells during immunotherapy and their number

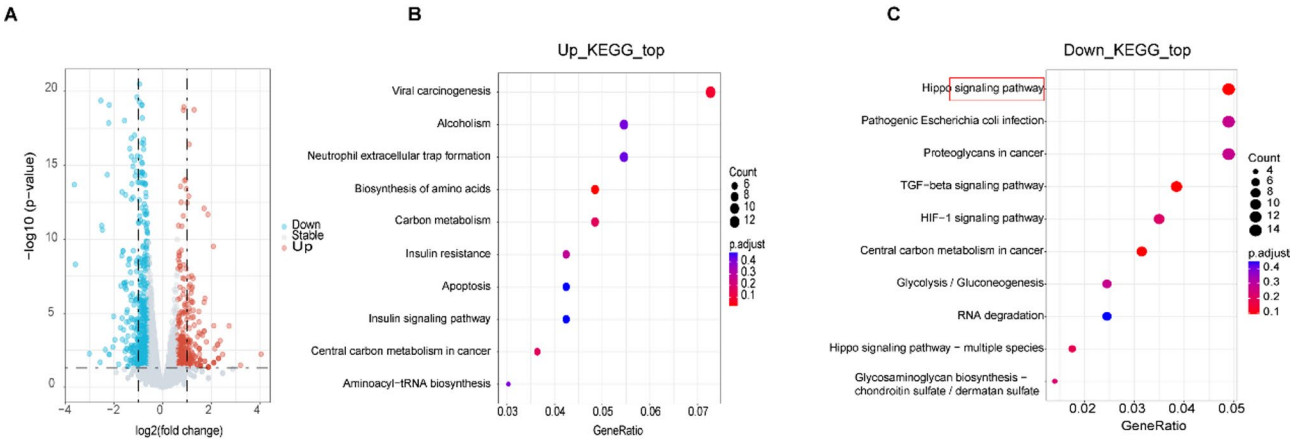

Fig. 7 Differentially expressed genes (DEGs) and pathways analyzed by bioinformatics. **(A)** Identification of differentially expressed genes. Volcano plot of gene expression profiles. Red/blue symbols classify the upregulated/downregulated genes according to the criteria:|logFC|> 2 and adjusted p-value. **(B)**Bubble Diagram exhibiting the most enriched KEGG pathways of up-regulated DEGs. **(C)** The same for **(B)** but for the down-regulated DEGs

and functional status largely determine their anti-tumor effects [21]. Macrophages regulated the immune response to pathogens and maintain tissue homeostasis [22]. DCs were specialized antigen-presenting cells with the unique ability to induce naïve T cell activation and effector differentiation [23]. The role of neutrophils in tumors was paradoxical: neutrophils were able to mediate a wide range of anti-tumor and pro-tumor activities, ranging from direct tumor cell killing to tumor cell proliferation, angiogenesis, metastasis and coordination of other immune responses [24]. Most malignant tumors reprogram macrophages into tumor-associated macrophages (TAMs) that drove tumor progression by enhancing proliferation, invasion, and metastatic dissemination [25]. Furthermore, TAMs contributed to therapeutic resistance against both conventional chemotherapy and immune checkpoint inhibitors [26]. Functional validation through PBMC coculture assays demonstrated that HECW1-knockdown GC cells increased $CD3^{+}CD8^{+}$ T cell proportions and enhanced IFN-γ/TNF-α secretion, suggesting its role in modulating T cell activity.

The Hippo signaling pathway mediates diverse cellular functions including immunomodulation, exerting both tumor-promoting effects and immunosuppressive functions through multiple mechanisms [27]. The Hippo-YAP axis and its downstream effectors YAP and transcriptional co-activator PDZ-binding motif (TAZ) were essential regulators of stem cell dynamics and tumorigenesis [28]. Aberrant activation of the YAP/TAZ signaling cascade commonly occurred in various malignancies. Previous research has found CD248 activation promoted non-small cell lung cancer metastasis through Hippo signaling stimulation [29], while RARγ knockdown inhibited Hippo-YAP signaling and suppressed colorectal cancer development [30]. To investigate the functional role of HECW1 in gastric carcinogenesis, our integrated analysis of public databases and transcriptomic sequencing results revealed that HECW1 may regulate the Hippo signaling pathway. To investigate the regulatory function of Hippo signaling in gastric cancer, we performed siRNA-mediated HECW1 knockdown, revealing its inhibitory effect on Hippo-YAP signaling. Rescue experiments demonstrated that YAP overexpression reversed the tumor-suppressive phenotypes caused by HECW1 depletion. Transcriptomic profiling integrated with in vitro validation confirmed HECW1-mediated Hippo-YAP pathway regulation. However, it remains unclear whether HECW1 directly ubiquitinates core components of the Hippo pathway (e.g., LATS1/2, MST1/2), and this requires further investigation. While current findings are limited by the absence of in vivo validation, future studies will clarify this mechanism using animal models.

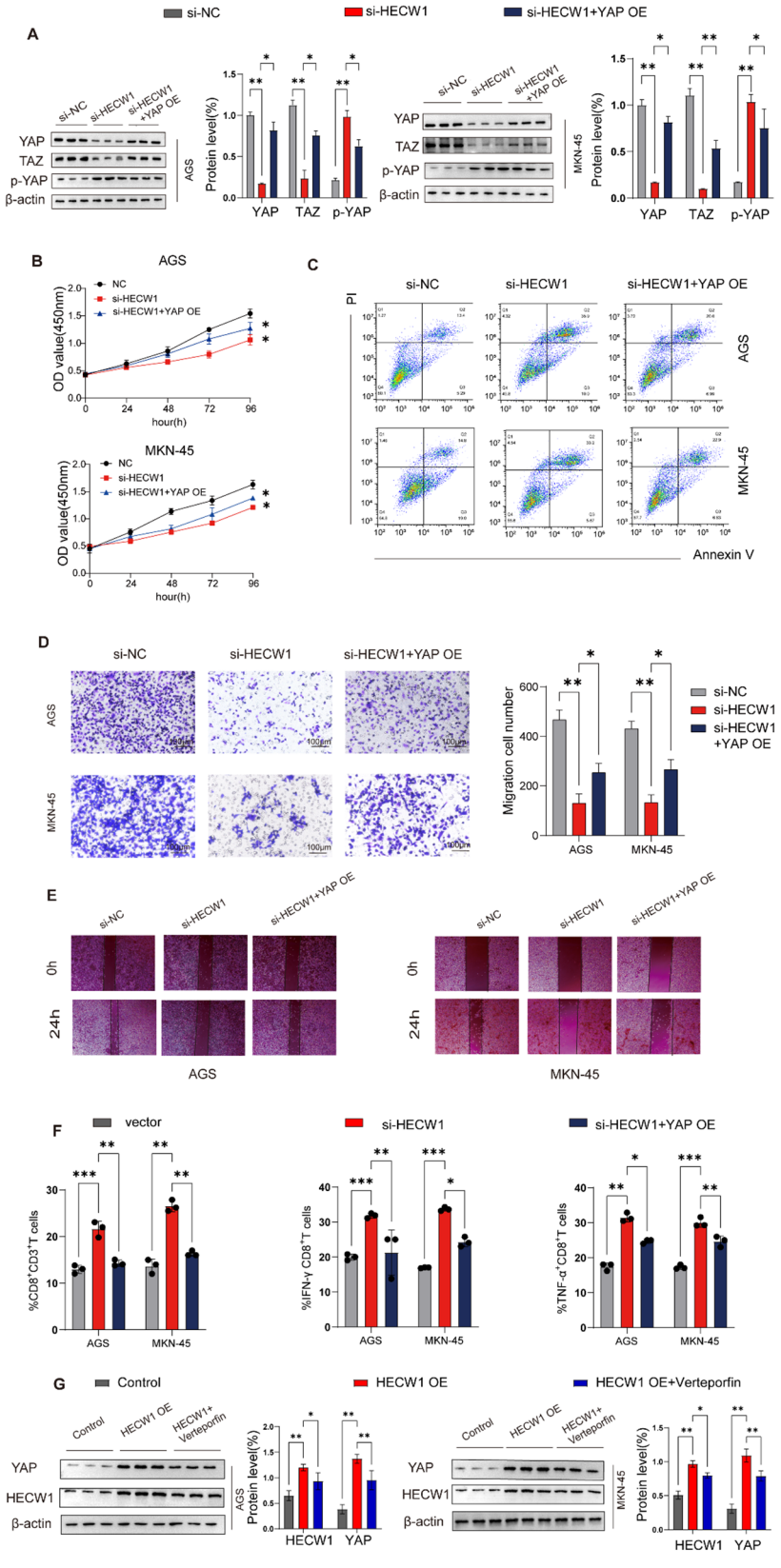

Fig. 8 (See legend on next page.)

(See figure on previous page.)

Fig. 8 Hippo pathway activation blocks the anti-tumor effects induced by HECW1 knockdown. **(A)** The protein level of YAP, TAZ, and p-YAP after silencing of HECW1 or silencing of HECW1 followed by addition of YAP overexpression plasmid and not (si-NC). **(B)** CCK-8 assays were performed to detect the proliferation of these transfected GC cells. **(C)** Functional rescue of apoptosis through Annexin V-FITC/PI dual-labeling assay. (**D**)Transwell assays of AGS and MKN-45 cells treated as indicated. **(E)**Wound healing assays were conducted to detect the invasion of these transfected GC cells. Transwell assays were stained by crystal violet solution. (**F**) Statistical quantitation of $CD3^+CD8^+$T cells, TNF-α^+CD8^+T cells, and IFN-γ^+CD8^+T cells. (G) The protein level of YAP after HECW1 overexpression with or without Verteporfin. Scale bar, **(D)** 100 μm, **(E)** 100 μm. $^*p < 0.05$, $^{**}p < 0.01$, $^{***}p < 0.001$

Conclusion

Elevated HECW1 expression is associated with poor prognosis and increased immune cell infiltration in GC. Mechanistically, HECW1 knockdown inhibits GC progression through suppression of cellular proliferation and migratory capacity, and induction of apoptosis mediated by activation of the Hippo signaling pathway. These findings highlight HECW1 as both a prognostic biomarker and a potential therapeutic target for precision oncology strategies in GC.

Supplementary Information

The online version contains supplementary material available at https://doi.org/10.1186/s12957-025-03866-3.

Supplementary Material 1

Acknowledgements

We are grateful for the open access to the following databases: the Tumor Immunoassay Resource (TIMER2.0) system, the Gene Expression Profiling Interaction Analysis (GEPIA2), the Kaplan-Meier-plotter, the cBioPortal, and the STRING database. Their valuable data have been crucial in supporting our research.

Author contributions

Z Yang: Writing – original draft, Methodology, Investigation, Formal analysis, Data curation, Conceptualization. P Zhou: Software, Methodology, Investigation. L Wang: Visualization, Methodology, Investigation. X Yang: Visualization, Methodology, Investigation. M Yang: Software, Formal analysis. J Xia: Writing – review & editing, Writing – original draft, Resources, Project administration, Investigation, Funding acquisition, Conceptualization.

Funding

This work was supported by Key Project of Scientific Research from Jiangsu Commission of Health (ZDB2020026); Wuxi Taihu Lake Talent Plan, Team in Medical and Health Profession; Wuxi Medical Key Discipline Construction Project, Medical Development Discipline; Postgraduate Research & Practice Innovation Program of Jiangsu Province (SJCX23_0690).

Data availability

Data is provided within the manuscript or supplementary information files.

Declarations

Ethical approval

The study was approved by the Ethics Committee of Wuxi No.2 People's Hospital [2023-Y-113], and all patients provided informed consent.

Consent for publication

Not applicable.

Competing interests

The authors declare no competing interests.

Received: 6 February 2025 / Accepted: 20 May 2025
Published online: 29 May 2025

References

1. Bray F, Laversanne M, Sung H, Ferlay J, Siegel RL, Soerjomataram I, Jemal A. Global cancer statistics 2022: GLOBOCAN estimates of incidence and mortality worldwide for 36 cancers in 185 countries. CA Cancer J Clin. 2024;74:229–63.
2. Dong D, Yu X, Xu J, Yu N, Liu Z, Sun Y. Cellular and molecular mechanisms of Gastrointestinal cancer liver metastases and drug resistance. Drug Resist Updat. 2024;77:101125.
3. Pao KC, Wood NT, Knebel A, Rafie K, Stanley M, Mabbitt PD, Sundaramoorthy R, Hofmann K, van Aalten DMF, Virdee S. Activity-based E3 ligase profiling uncovers an E3 ligase with esterification activity. Nature. 2018;556:381–5.
4. Sampson C, Wang Q, Otkur W, Zhao H, Lu Y, Liu X, Piao HL. The roles of E3 ubiquitin ligases in cancer progression and targeted therapy. Clin Transl Med. 2023;13:e1204.
5. Zheng N, Shabek N. Ubiquitin ligases: structure, function, and regulation. Annu Rev Biochem. 2017;86:129–57.
6. Miyazaki K, Fujita T, Ozaki T, Kato C, Kurose Y, Sakamoto M, Kato S, Goto T, Itoyama Y, Aoki M, Nakagawara A. NEDL1, a novel ubiquitin-protein isopeptide ligase for dishevelled-1, targets mutant superoxide dismutase-1. J Biol Chem. 2004;279:11327–35.
7. Li Y, Ozaki T, Kikuchi H, Yamamoto H, Ohira M, Nakagawara A. A novel HECT-type E3 ubiquitin protein ligase NEDL1 enhances the p53-mediated apoptotic cell death in its catalytic activity-independent manner. Oncogene. 2008;27:3700–9.
8. Lin Y, Gong H, Liu J, Hu Z, Gao M, Yu W, Liu J. HECW1 induces NCOA4-regulated ferroptosis in glioma through the ubiquitination and degradation of ZNF350. Cell Death Dis. 2023;14:794.
9. Xu Z, Guo Y, Wang L, Cui J. HECW1 restrains cervical cancer cell growth by promoting DVL1 ubiquitination and downregulating the activation of Wnt/β-catenin signaling. Exp Cell Res. 2024;435:113949.
10. Li T, Fu J, Zeng Z, Cohen D, Li J, Chen Q, Li B, Liu XS. TIMER2.0 for analysis of tumor-infiltrating immune cells. Nucleic Acids Res. 2020;48:W509–14.
11. Li T, Fan J, Wang B, Traugh N, Chen Q, Liu JS, Li B, Liu XS. TIMER: A web server for comprehensive analysis of Tumor-Infiltrating immune cells. Cancer Res. 2017;77:e108–10.
12. Győrffy B. Integrated analysis of public datasets for the discovery and validation of survival-associated genes in solid tumors. Innov (Camb). 2024;5:100625.
13. Tang Z, Kang B, Li C, Chen T, Zhang Z. GEPIA2: an enhanced web server for large-scale expression profiling and interactive analysis. Nucleic Acids Res. 2019;47:W556–60.
14. de Bruijn I, Kundra R, Mastrogiacomo B, Tran TN, Sikina L, Mazor T, Li X, Ochoa A, Zhao G, Lai B, et al. Analysis and visualization of longitudinal genomic and clinical data from the AACR project GENIE biopharma collaborative in cBioPortal. Cancer Res. 2023;83:3861–7.
15. Conesa A, Madrigal P, Tarazona S, Gomez-Cabrero D, Cervera A, McPherson A, Szcześniak MW, Gaffney DJ, Elo LL, Zhang X, Mortazavi A. A survey of best practices for RNA-seq data analysis. Genome Biol. 2016;17:13.
16. Chandrashekar DS, Karthikeyan SK, Korla PK, Patel H, Shovon AR, Athar M, Netto GJ, Qin ZS, Kumar S, Manne U, et al. UALCAN: an update to the integrated cancer data analysis platform. Neoplasia. 2022;25:18–27.
17. Lu C, Ning G, Si P, Zhang C, Liu W, Ge W, Cui K, Zhang R, Ge S. E3 ubiquitin ligase HECW1 promotes the metastasis of non-small cell lung cancer cells through mediating the ubiquitination of Smad4. Biochem Cell Biol. 2021;99:675–81.
18. Liu Y, Liu Z, Yang Y, Cui J, Sun J, Liu Y. The prognostic and biology of tumour-infiltrating lymphocytes in the immunotherapy of cancer. Br J Cancer. 2023;129:1041–9.
19. Lin B, Du L, Li H, Zhu X, Cui L, Li X. Tumor-infiltrating lymphocytes: warriors fight against tumors powerfully. Biomed Pharmacother. 2020;132:110873.
20. Solinas C, Pusole G, Demurtas L, Puzzoni M, Mascia R, Morgan G, Giampieri R, Scartozzi M. Tumor infiltrating lymphocytes in Gastrointestinal tumors:

controversies and future clinical implications. Crit Rev Oncol Hematol. 2017;110:106–16.
21. Wang Q, Qin Y, Li B. CD8(+) T cell exhaustion and cancer immunotherapy. Cancer Lett. 2023;559:216043.
22. Mehla K, Singh PK. Metabolic regulation of macrophage polarization in Cancer. Trends Cancer. 2019;5:822–34.
23. Patente TA, Pinho MP, Oliveira AA, Evangelista GCM, Bergami-Santos PC, Barbuto JAM. Human dendritic cells: their heterogeneity and clinical application potential in Cancer immunotherapy. Front Immunol. 2018;9:3176.
24. Mackey JBG, Coffelt SB, Carlin LM. Neutrophil Maturity in Cancer. *Front Immunol* 2019, 10:1912.
25. Ngambenjawong C, Gustafson HH, Pun SH. Progress in tumor-associated macrophage (TAM)-targeted therapeutics. Adv Drug Deliv Rev. 2017;114:206–21.
26. Pu Y, Ji Q. Tumor-Associated macrophages regulate PD-1/PD-L1 immunosuppression. Front Immunol. 2022;13:874589.
27. Wang Z, Wang F, Ding XY, Li TE, Wang HY, Gao YH, Wang WJ, Liu YF, Chen XS, Shen KW. Hippo/YAP signaling choreographs the tumor immune microenvironment to promote triple negative breast cancer progression via TAZ/IL-34 axis. Cancer Lett. 2022;527:174–90.
28. Wu H, Che YN, Lan Q, He YX, Liu P, Chen MT, Dong L, Liu MN. The multifaceted roles of Hippo-YAP in cardiovascular diseases. Cardiovasc Toxicol 2024.
29. Wu J, Zhang Q, Yang Z, Xu Y, Liu X, Wang X, Peng J, Xiao J, Wang Y, Shang Z, et al. CD248-expressing cancer-associated fibroblasts induce non-small cell lung cancer metastasis via Hippo pathway-mediated extracellular matrix stiffness. J Cell Mol Med. 2024;28:e70025.
30. Guo PD, Lu XX, Gan WJ, Li XM, He XS, Zhang S, Ji QH, Zhou F, Cao Y, Wang JR, et al. RARγ downregulation contributes to colorectal tumorigenesis and metastasis by derepressing the Hippo-Yap pathway. Cancer Res. 2016;76:3813–25.

Publisher's note